



## Therapeutic impact of stachyose on hyperlipidaemia caused by a high-fat diet in mice as revealed by gut microbiota and metabolomics

Wensen Zhang<sup>a</sup>, Na Cui<sup>a</sup>, Fazhi Su<sup>a</sup>, Yanping Sun<sup>a</sup>, Biao Li<sup>a</sup>, Zhihong Zhang<sup>a</sup>, Yuanning Zeng<sup>b</sup>, Wei Guan<sup>a</sup>, Bingyou Yang<sup>a</sup>, Qihong Wang<sup>b,\*</sup>, Haixue Kuang<sup>a,\*</sup>

<sup>a</sup> Key Laboratory of Basic and Application Research of Beiyao (Heilongjiang University of Chinese Medicine), Ministry of Education, 24 Heping Road, Xiangfang District, Harbin, 150040, China

<sup>b</sup> Guangdong Engineering Technology Research Center for Standardized Processing of Chinese Materia Medica (Guangdong Pharmaceutical University, School of Chinese Materia Medica), Guangdong, 510006, China

### ARTICLE INFO

Handling Editor: Dr. Yeonhwa Park

**Keywords:**  
Metabolomics  
Stachyose  
Hyperlipidaemia  
High-fat diet  
Gut microbiota

### ABSTRACT

Hyperlipidaemia, which is characterized by an excess of lipids or fats in the bloodstream, is a high-risk factor and critical indicator of many metabolic diseases. This study used 16 S rRNA gene sequencing and metabolomics to determine that stachyose (ST) has a therapeutic effect and is a mechanism of hyperlipidaemia. These results show that ST significantly attenuated high-fat diet-induced weight gain and fat deposition while also adjusting the gut microbial composition. Untargeted serum metabolomics identified 12 biomarkers, which suggests that ST may function by regulating metabolic pathways. These results highlight the potential of ST in treating hyperlipidaemia and provides directions for future research including an in-depth investigation of the bioactive components, dosage, and treatment strategies of ST.

### 1. Introduction

Due to the long-term intake of high-fat and high-calorie foods, the body's blood lipid metabolism becomes disordered and metabolic-related diseases can occur, such as diabetes (Liu et al., 2022), hyperlipidaemia, obesity (Chai et al., 2022), and cardiovascular diseases (Yoo et al., 2021). Among these diseases, hyperlipidaemia is the most common symptom of dyslipidaemia with weight gain and blood lipid changes as characteristic parameters (Tietge, 2014). Specific manifestations are elevated serum low-density lipoprotein cholesterol (LDL-C), triglycerides (TG), and total cholesterol (TC) levels and reduced high-density lipoprotein cholesterol (HDL-C) levels (Yu et al., 2022a,b). Commonly, alanine aminotransferase (ALT) and aspartate aminotransferase (AST) activities in serum are used as reliable markers for liver damage. When hepatocytes are damaged, these enzymes can leach out into the bloodstream and lead to a significant activity increase in the serum (Dong et al., 2019). Hyperlipidaemia is one of the critical risk factors for cardiovascular disease can easily lead to severe illnesses such as atherosclerosis (Nasioudis et al., 2019), coronary heart disease, and cerebrovascular disease (Tóth et al., 2020). Although common blood

lipid-lowering drugs, such as simvastatin and lovastatin, have excellent effects, long-term use of these drugs will cause symptoms such as gastrointestinal discomfort. Therefore, many scientists are working to develop effective antihyperlipidaemic drugs and antihyperlipidaemic active substances derived from natural products.

Stachyose (ST) is a natural product that can be extracted from various plants, such as cucumbers (Zhao et al., 2016), strawberries (Olsson et al., 2004), and watermelons (Jovanovic-Malinovska et al., 2015). Specifically, is a high-quality dietary fibre and prebiotic (He et al., 2020). As a classic prebiotic, ST is proven to promote the growth of beneficial intestinal bacteria, inhibit pathogenic bacteria, and improve glucose metabolism (Liu et al., 2019). In addition, ST can also enhance the absorption of soybean genistein and tea polyphenols in mice (Li et al., 2016a,b; Lu et al., 2017). Overall, disease resistance is improved and immunity strengthened, which should be widely used in medicine. In addition, compared with traditional drugs, ST, as a natural product, has fewer side effects, low toxicity, and no adverse effects on the liver and kidneys, which makes it more suitable for long-term use.

Combined metabolomics and gut microbiota analysis has become a common approach in addressing metabolic disease (Yu et al., 2022a,b).

\* Corresponding author.

\*\* Corresponding author.

E-mail addresses: [qhwang668@sina.com](mailto:qhwang668@sina.com) (Q. Wang), [hxkuang@hljucm.net](mailto:hxkuang@hljucm.net) (H. Kuang).

Metabolomics is the study of the overall changes in metabolites in organisms, which can reveal changes in the metabolic process of organisms and help people understand the physiological state, metabolic pathways, and mechanisms of metabolic disorders of organisms. The gut microbiota is the microbial community in the gut that can help to understand intestinal microbiota composition and abundance changes and also the relationship between the gut microbiota and health. The combined analysis of these two methods can provide a more comprehensive understanding of the metabolic state and biological mechanisms in organisms, and thereby help people better understand the occurrence and development of metabolic diseases and explore new ways of prevention and treatment.

Hyperlipidaemia is a widespread health problem closely related to serious health problems such as cardiovascular disease. Although many treatments for hyperlipidaemia exist, including medications and lifestyle interventions, finding more effective treatments remains an urgent need. Therefore, this study is essential in exploring the potential role of ST in treating hyperlipidaemia. This study characterized the beneficial effects of ST on hyperlipidaemia through metabolomics combined with intestinal microbiome analysis.

## 2. Materials and methods

### 2.1. Chemicals and reagents

We purchased stachyose from Yuan Ye Bio (Lot: Y1309H72158). We used TC, TG, LDL-C, HDL-C, ALT, and AST kits from Nanjing Jiancheng Institute of Biological Engineering (batch numbers: 20220830, 20220830, 20220830, 20220830, 20220827, and 20220826). Mass spectrometry grade formic acid and acetonitrile were purchased from Thermo Fisher (batch number: 205178, 218758, 205187).

### 2.2. Animals and ethics statement

Specific pathogen-free (SPF)-grade male C57BL/6 mice (6–8 weeks old, purchased from Guangdong Medical Experimental Animal Center, China, licence number SCXK (Guangdong) 2022-0002) were raised under standard conditions (12/12 h of alternating light and dark, temperature 20–24 °C, and relative humidity 40–60%). After a week of adaptive feeding and drinking water, the mice were randomly divided into 5 groups (control group, model group, ST-H group, ST-M group, and ST-L group) (n = 8).

### 2.3. Establishment of the hyperlipidaemia model

We provided a control diet (purchased from Guangdong Medical Experimental Animal Center, licence number: Guangdong Provincial Feeding Certificate (2019) 05073) and a high-fat diet (purchased from Jiangsu Xieli Pharmaceutical Biotechnology Co., Ltd., batch number: XTHF45, ingredients: crude protein 22.5%, crude fat 24.2%, crude fibre 3.2%, crude ash 5.6%, calcium 1.2%, and total phosphorus 0.8%) for the other groups. The control group mice were fed a dietary formula of 18.5% protein, 4.6% fat, 58.9% carbohydrates, 3.2% crude fibre, 6.8% ash, 1.28% calcium, and 0.92% phosphorus. We conducted the experiment under the national and EU guidelines on the handling and use of experimental animals and the research and protocol were approved by the Ethics Committee of Heilongjiang University of Chinese Medicine (approval number: 2019121101).

Blood was collected from the tail tip of the mice on Day 28, and blood lipid levels (TC, TG, HDL-C, and LDL-C) were measured. All groups were orally administered the same amount of ST-H (300 mg/kg), ST-M (150 mg/kg), and ST-L (75 mg/kg) until the 63rd day. The control and model groups were orally administered saline, and each animal's body weight was measured weekly during this period. At the end of the test, blood was collected, the liver tissue was and epididymal fat was weighed, and tissue samples were preserved as needed while fasting for 12 h.

### 2.4. Biochemical analysis of blood samples

The collected blood was refrigerated at a temperature of 4 °C for 30 min and then centrifuged (Hunan Xiangyi Company, China) at 3500 rpm/min for 15 min to gather the serum. Then, we determined the AST, ALT, TC, TG, LDL-C, and HDL-C levels in the serum.

### 2.5. Histopathological examination

Mouse liver and epididymal adipose tissue were analysed using haematoxylin-eosin (H&E) staining. A portion of the mouse liver and epididymal fat was fixed in a 4% paraformaldehyde solution, embedded in paraffin, and stained with H&E. A microscope (Nikon Eclipse Ci-L, Japan) was used at 400 × magnification to observe the area and capture sample images.

### 2.6. Metabolomics analysis

#### 2.6.1. Blood sample preparation

We added the serum (50 µL) to acetonitrile (150 µL) and centrifuged it (Hunan Xiangyi Company, China) at 13,000 rpm/min at 4 °C for 10 min. We evaporated the supernatant and dissolved it in 50% acetonitrile. After high-speed centrifugation (13,000 rpm/min), the supernatant was collected for testing. The solution (10 µL) was extracted from each sample and mixed with all samples as a quality control (QC) sample (Cui et al., 2023).

#### 2.6.2. MS conditions

All chromatographic analyses were performed on an ultrahigh-performance liquid phase (Dionex Ultimate 3000, USA) tandem electrostatic field orbitrap high-resolution mass spectrometer (Thermo Orbitrap Fusion, USA). In this study, serum metabolomics were determined using a Waters ACQUITY UPLC HSS T3 (1.8 µm, 2.1 × 100 mm) column. The injection flow rate was 0.4 mL/min.

Both positive and negative ion modes used an H-ESI ion source with an ionization voltage of 3.5 kV and 2.8 kV, an Ion Transfer Tube Temp at 300 °C, a Vaporizer Temp at 320 °C, Sheath gas at 20 Arb, Auxiliary gas at 6 Arb, and Mass Range at 100–1000 m/z. Fragment energies were 15%, 25%, and 35% with a resolution of 15,000, and the Dynamic rendition time was 6 s.

Mobile phases A was water, 0.1% formic acid and phase B was acetonitrile. The mobile phase B gradients were as follows: 2%–35% (1–4 min), 35%–100% (4–13 min), 100%–100% (13–15.5 min), and 100%–2% (15.5–19 min) for the analysis of metabolomics. The stability of the investigation was continuously monitored by systematically analysing QC samples every 10 (Cui et al., 2023).

#### 2.6.3. Reliability of the metabolomics platform

High-quality data were important in the metabolomics study. The relative standard deviation (RSD) of all ions detected in QC samples was calculated to evaluate the stability of the instrument and the analytical method. For the contents of 12 biomarkers in 4 QCs, the RSD range was 1.15%–4.93%, which indicated that the analytical system and method could be operated with relatively high reproducibility and stability.

#### 2.6.4. Multivariate data analysis

The Compound Discover 3.2 platform (Thermo, USA) was used to obtain potential and critical annotations from the original centroid data file obtained by Orbitrap Fusion Tune. Principal component analysis (PCA) plots and orthogonal partial least squares discriminant analysis (OPLS-DA) plots were obtained by SIMCA-P (version 14, Sweden). Metabolite annotation was made by searching MS and MS/MS information against HMDB. The mass error tolerance was set at 5 ppm. The *t*-test value was significantly different when lower than 0.05.

## 2.7. 16 S sequencing and analysis

### 2.7.1. DNA extraction and PCR amplification

The total microbial genomic DNA was extracted from colon content samples using the PF Mag-Bind Stool DNA Kit (Omega Biotek, GA, USA) according to the manufacturer's instructions. The quality and concentration of DNA were determined by 1.0% agarose gel electrophoresis and a NanoDrop® ND-2000 spectrophotometer (Thermo Scientific Inc., USA) and stored at  $-80^{\circ}\text{C}$  for further use. The hypervariable region V3-V4 of the bacterial 16 S rRNA gene was amplified by an ABI GeneAmp® 9700 PCR (California, USA State ABI) thermal cycler using the primer pair 338 F (5'-ACTCTACGGGAGGAGCAGCAG-3') and 806 R (5'-GGACTACHVGGGTWTCTAAT-3') (Liu et al., 2016). The PCR mixture included 4  $\mu\text{L}$  5  $\times$  Fast Pfu buffer, 2  $\mu\text{L}$  2.5 mM dNTPs, 0.8  $\mu\text{L}$  forward and reverse primers (5  $\mu\text{M}$ ), 0.4  $\mu\text{L}$  Fast Pfu polymerase, 10 ng template DNA, and ddH<sub>2</sub>O at a final volume of 20  $\mu\text{L}$ . The PCR amplification cycle conditions were as follows: initial denaturation at  $95^{\circ}\text{C}$  for 3 min, denaturation at  $95^{\circ}\text{C}$  for 30 s, annealing at  $55^{\circ}\text{C}$  for 30 s, extension at  $72^{\circ}\text{C}$  for 45 s, and 27 cycles of single extension at  $72^{\circ}\text{C}$  for 10 min with an end at  $4^{\circ}\text{C}$ . All samples were amplified in triplicate. PCR products were extracted and purified from 2% agarose gel. Then, quantification was performed using a Quantus™ fluorometer (Promega, USA).

### 2.7.2. Data processing

Raw FASTQ files were demultiplexed using an in-house Perl script and then quality filtered via fastp version 0.19.6 (Chen et al., 2018) and merged via FLASH version 1.2.11 (Magoč and Salzberg, 2011) to meet the following criteria. (i) Truncate 300 bp reads at any site with an average quality score  $<20$  on a 50 bp sliding window, discard truncated reads shorter than 50 bp, and discard reads containing ambiguous characters. (ii) Assemble based on overlapping sequences for only overlapping sequences longer than 10 bp. The maximum mismatch ratio in the overlapping area was 0.2, and reads that could not be assembled were discarded. (iii) Samples were distinguished based on barcodes and

primers, and sequence directions were adjusted so that barcodes were accurately matched and primers were matched with 2 nucleotide mismatches. The optimized sequences were then clustered into operational taxonomic units (OTUs) using UPARSE 11 with a sequence similarity of 97% (Edgar, 2013). The most abundant sequence for each OTU was selected as the representative sequence.

## 2.8. Statistical analysis

All obtained data are expressed as the mean  $\pm$  standard deviation. One-way analysis of variance (ANOVA) with Tukey's post hoc test was used for intergroup comparisons using GraphPad Prism 7 software (GraphPad Software Inc., San Diego, CA, USA). The data significance was determined by considering a  $p < 0.05$  as representative of a significant difference, while  $p < 0.01$  was considered to be indicative of a highly significant difference. GraphPad Prism 7 software was used to plot histograms. This experiment was repeated twice, and the results were stable.

## 3. Results

### 3.1. Effects of ST on body weight and liver index in HFD mice

After two weeks on the HFD, all experimental groups showed significant differences in body weight, which confirmed an effect of the treatments. However, after the subsequent intervening ST, differences in the body weight of the experimental mice emerged. The body weight of the mice in the ST-H group was significantly lower than that in the model group ( $p < 0.05$ , Fig. 1A). Statistical analysis of mouse body weights obtained during the experiments showed consistently similar results (Fig. 1B). The liver index of the model group was significantly higher than that of the control group ( $p < 0.01$ ). However, the ST-H and ST-M groups ( $p < 0.05$ ) showed a significant decrease compared to the model group. We observed no significant differences in the liver index in

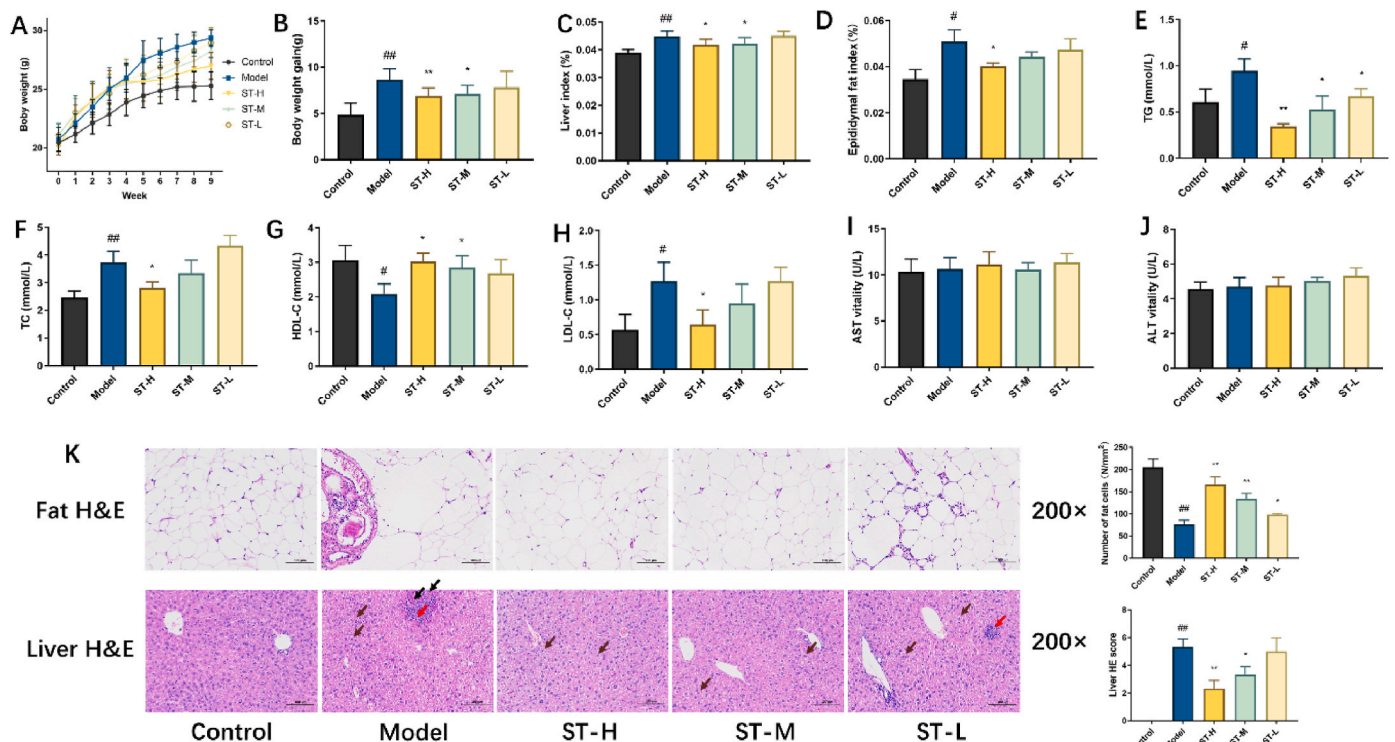


**Fig. 1.** Effects of ST on body weight, organs, and blood lipid levels in hyperlipidemia mice. (A) Body weight. (B) Weight gain. (C) Liver index. (D) Epididymal fat index. (E) TG levels. (F) TC levels. (G) HDL-C levels. (H) LDL-C levels. (I) AST levels. (J) ALT levels. (K) H&E staining of liver and epididymal fat. Each value represents the mean  $\pm$  SD ( $n = 7$ ). ## $p < 0.01$  or # $p < 0.05$ , compared with the control group; \* $p < 0.05$  or \*\* $p < 0.01$ , compared with the model group.

the ST-L group (Fig. 1C). In the epididymal fat index, the model group was significantly higher than the control group ( $p < 0.05$ ). However, the ST-H group ( $p < 0.05$ ) showed a significant decrease compared with the model group. Notably, we observed no significant difference in the epididymal fat index between the ST-L and ST-M groups (Fig. 1D). These findings suggest that the effect of ST on HFD is dose dependent.

### 3.2. Effects of ST on visceral adipose tissue and blood lipids in HFD mice

We analysed the morphological changes of H&E staining in adipose and liver tissue. We found significant changes in the number and size of visible adipocytes after H&E staining in photographic analysis at the same magnification of the field of view. In addition, large cell variability was found in the control group, and the model group and the experimental group under ST intervention showed dose-dependent and similar viability when counting the number of cells. In the liver tissue, H&E staining of liver sections in the model group showed more round lipid droplets and more significant vesicular fatty degeneration than in the control group. There was mild focal infiltration of a small number of lymphocytes. At the end of the trial, treatment in the ST-H group significantly reduced fatty liver and lipid deposition, and hepatic lobular and confluent lesions were alleviated (Fig. 1K). Furthermore, the lipid profile showed that additional intervention in the ST-H group significantly rescued HFD-associated increases in lipid TG, TC, and LDL-C and decreased HDL-C (Fig. 1E-H). There was no significant change in AST and ALT, which proved that ST has no toxicity to mouse liver and is safe and reliable.

### 3.3. Effect of ST on the metabolomics in HFD mice

PCA of mouse serum metabolic profiles in different groups revealed distinct separation between the control and model groups. However, partial overlap was observed among the ST-H, ST-M, and ST-L groups (Fig. 2A and B). Subsequently, using the PLS-DA pattern recognition method with screening conditions  $VIP > 1$  and  $p < 0.05$ , we identified 12 common differentially abundant metabolites including 7 in positive ion modes and 5 in negative ion modes (Fig. 2C and D). These results demonstrated significant differences in the metabolites of mice fed a HFD after ST intervention compared to those without ST intervention, and data reliability was high (Fig. 2A and C). Specifically, under the ST intervention, 4 differentially abundant metabolites, histamine, glycocholic acid, glycitein, and erucic acid, reversed the relatively increased abundance induced by a HFD in a dose-dependent manner. In contrast, the 8 distinct metabolites of vitamin A, threonic acid, taurine, serotonin, phenylalanine, PC(18:3(9Z,12Z,15Z)/18:2(9Z,12Z)), oleic acid, and hippuric acid corrected the HFD-induced relative decrease in abundance in a dose-dependent manner (Table 1). The fold change and  $p$  value changes among all groups are shown in Fig. 2E. According to the Kyoto Encyclopedia of Genes and Genomes (KEGG), we enriched potential pathways of different metabolites. Five possible metabolic pathways were screened by parameters such as  $p$  value and impact including phenylalanine metabolism, phenylalanine, tyrosine and tryptophan biosynthesis, primary bile acid biosynthesis, linoleic acid metabolism, and taurine and hypotaurine metabolism (Fig. 2F).

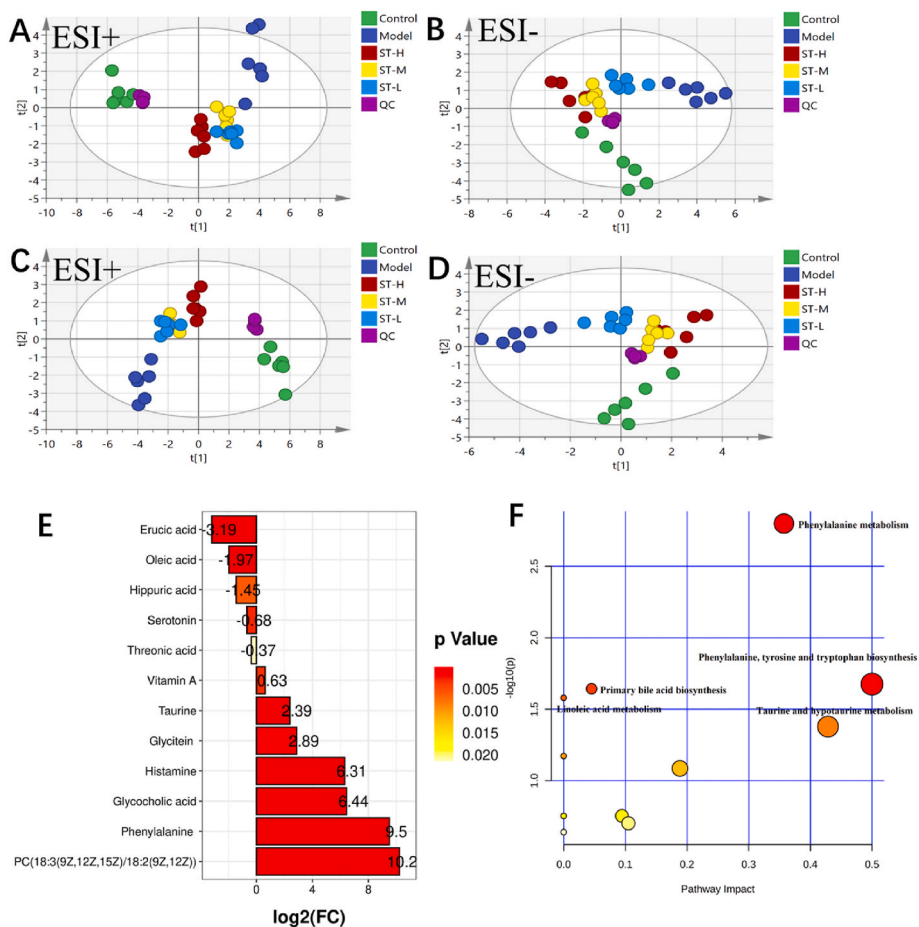


**Fig. 2.** Effect of ST intervention on serum metabolites. (A) PCA plot (ESI+). (B) PCA plot (ESI-). (C) PLS-DA graph (ESI+). (D) PLS-DA graph (ESI-). (E) Histograms of FC and  $p$  values of metabolites. (F) KEGG metabolic pathway analysis.

**Table 1**

Changes in the levels of metabolites; a, represent compared with the control group. b, represent compared with the model group.

| Metabolite                        | HMDB ID | Adducts | Formula   | m/z      | RT (min) | Ion mode | Mass error (ppm) | a     | b    | b    | b    |
|-----------------------------------|---------|---------|---|----------|----------|----------|------------------|-------|------|------|------|
|                                   |         |         |   |          |          |          |                  | Model | ST-H | ST-M | ST-L |
| Vitamin A                         | 305     | M + H   | C <sub>20</sub> H <sub>30</sub> O                 | 286.2284 | 6.17     | +        | -4.38            | ↑     | ↓    | ↓    | ↓    |
| Threonic acid                     | 943     | M-Na    | C <sub>4</sub> H <sub>8</sub> O <sub>5</sub>      | 136.0364 | 0.65     | -        | -2.54            | ↑     | ↓    | ↓    | ↓    |
| Taurine                           | 251     | M + Na  | C <sub>2</sub> H <sub>7</sub> NO <sub>3</sub> S   | 125.0154 | 0.63     | +        | 4.72             | ↑     | ↓    | ↓    | ↓    |
| Serotonin                         | 259     | M + H   | C <sub>10</sub> H <sub>12</sub> N <sub>2</sub> O  | 176.0967 | 0.86     | +        | 1.74             | ↑     | ↓    | ↓    | ↓    |
| Phenylalanine                     | 159     | M + H   | C <sub>9</sub> H <sub>11</sub> NO <sub>2</sub>    | 165.0798 | 1.90     | +        | 4.73             | ↑     | ↓    | ↓    | ↓    |
| PC(18:3(9Z,12Z,15Z)/18:2(9Z,12Z)) | 8204    | M + H   | C <sub>44</sub> H <sub>78</sub> NO <sub>8</sub> P | 779.5495 | 14.72    | +        | 3.82             | ↑     | ↓    | ↓    | ↓    |
| Oleic acid                        | 207     | M-Na    | C <sub>18</sub> H <sub>34</sub> O <sub>2</sub>    | 282.2552 | 13.88    | -        | -2.39            | ↑     | ↓    | ↓    | ↓    |
| Histamine                         | 870     | M + H   | C <sub>5</sub> H <sub>9</sub> N <sub>3</sub>      | 111.0801 | 0.52     | +        | 3.92             | ↓     | ↑    | ↑    | ↑    |
| Hippuric acid                     | 714     | M-H     | C <sub>9</sub> H <sub>9</sub> NO <sub>3</sub>     | 179.0572 | 4.43     | -        | -4.41            | ↑     | ↓    | ↓    | ↓    |
| Glycocholic acid                  | 138     | M-H     | C <sub>26</sub> H <sub>43</sub> NO <sub>6</sub>   | 465.3084 | 6.71     | -        | -1.45            | ↓     | ↑    | ↑    | ↑    |
| Glycitein                         | 5781    | M + H   | C <sub>16</sub> H <sub>12</sub> O <sub>5</sub>    | 284.0714 | 6.02     | +        | -0.35            | ↓     | ↑    | ↑    | ↑    |
| Erucic acid                       | 2068    | M-H     | C <sub>22</sub> H <sub>42</sub> O <sub>2</sub>    | 338.3175 | 15.90    | -        | -2.8             | ↓     | ↑    | ↑    | ↑    |

### 3.4. Effect of ST on the gut microbiota in HFD mice

As shown in Fig. 3A, the curve gradually flattens out, which indicates a reasonable amount of sample sequencing data asymptotically. In addition, the rank-abundance curves were long-spanning and flattened on the horizontal axis, which indicated species richness and a homogeneous composition (Fig. 3B). We identified 215 operational taxonomic units (OTUs) in the intestinal microbiota of all groups based on the >97% similarity between sequences (Fig. 3C). In terms of the Chao1 index, Shannon index, and Simpson index (Fig. 3D–F), the model group showed significantly lower species diversity than the control group. Furthermore, the ST-H group exhibited much higher species diversity than the model group, and ST enhanced the richness and diversity of the gut microbiome.

At the phylum level, we identified 10 bacterial phyla from the 16 S rRNA gene sequences. In the analysis of the taxonomic composition of microbial species, the relative abundance of species among groups responded differently to changes in the abundance of the dominant gut microbiome at the phylum level as a result of the HFD and ST intervention. These results showed that ST tended to downregulate *Firmicutes* and F/B ratios. ST-H performed relatively better than ST-M and ST-L (Fig. 4A). The heatmap of the main species in the phylum-based gut microbiota analysis revealed the abundance variation of the dominant

gut microbiome composition at the phylum level for each experimental group (Fig. 4B). At the genus level, the ST-H group greatly upregulated the relative abundance of *Ileibacterium* compared with the model group (Fig. 4C). The heatmap of the main species in the genus-based gut microbiota analysis revealed the abundance variation of the dominant gut microbiome composition at the genus level for each experimental group (Fig. 4D).

Using PCoA analysis of unweighted UniFrac distances, we assessed gut microbiota diversity in HFD-fed mice. The results (Fig. 5A and B) demonstrated significant differences between the control and model groups and indicated dysregulation of the gut microbiome in HFD-fed mice. Interestingly, there was no overlap between the ST-H and model groups, which suggests that ST-H had a therapeutic effect on HFD-fed mice. Similar observations were obtained from NMDS analysis (Fig. 5C). To further validate these findings, we conducted a MetaStats analysis of the sequencing data in PCA plots (Fig. 5D and E) consistent with the results from PCoA and NMDS analyses. To support our findings, we performed PLS-DA analysis (Fig. 5F), which showed better population dispersion between groups and further confirmed the observed significant differences. We generated a heatmap to visually represent the calculated unweighted UniFrac distance between samples (Fig. 5G). This heatmap highlighted that HFD-fed mice in the ST-H group exhibited a more pronounced treatment effect than those in the ST-M and ST-L

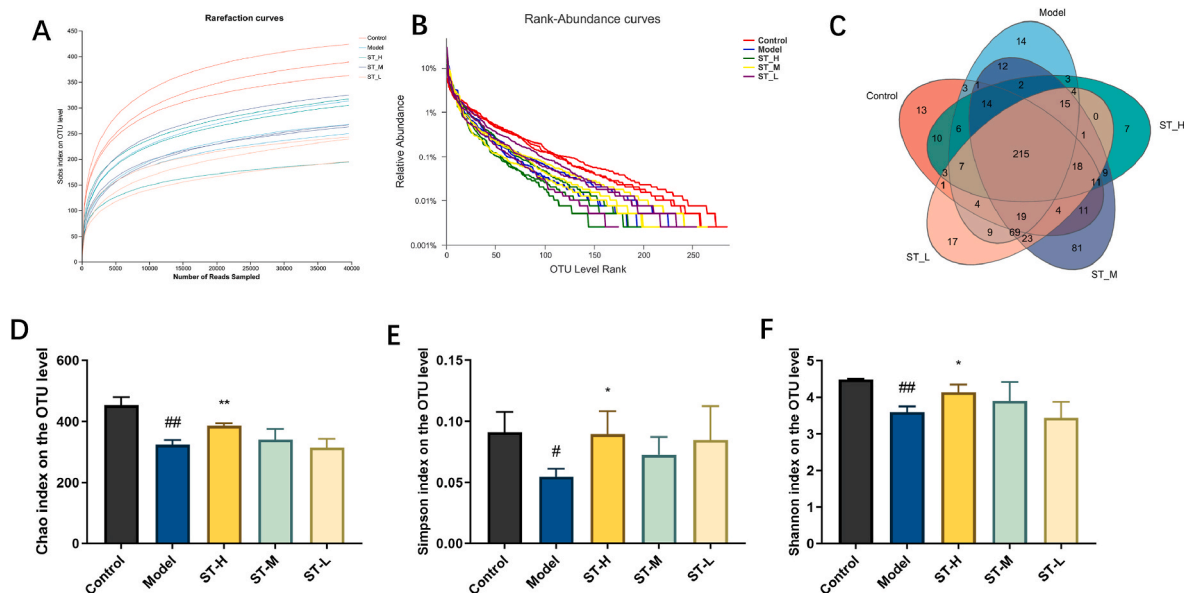


**Fig. 3.** Effect of ST on the richness and diversity of fecal microbiota in mice. (A) Rarefaction curves. (B) Rank abundance curves. (C) OTU Venn diagram. (D) Chao index. (E) Simpson index. (F) Shannon index. Each value represents the mean  $\pm$  SD ( $n = 3$ ). # $p < 0.05$ , ## $p < 0.01$  compared with the control group; \* $p < 0.05$ , \*\* $p < 0.01$  compared with the model group.

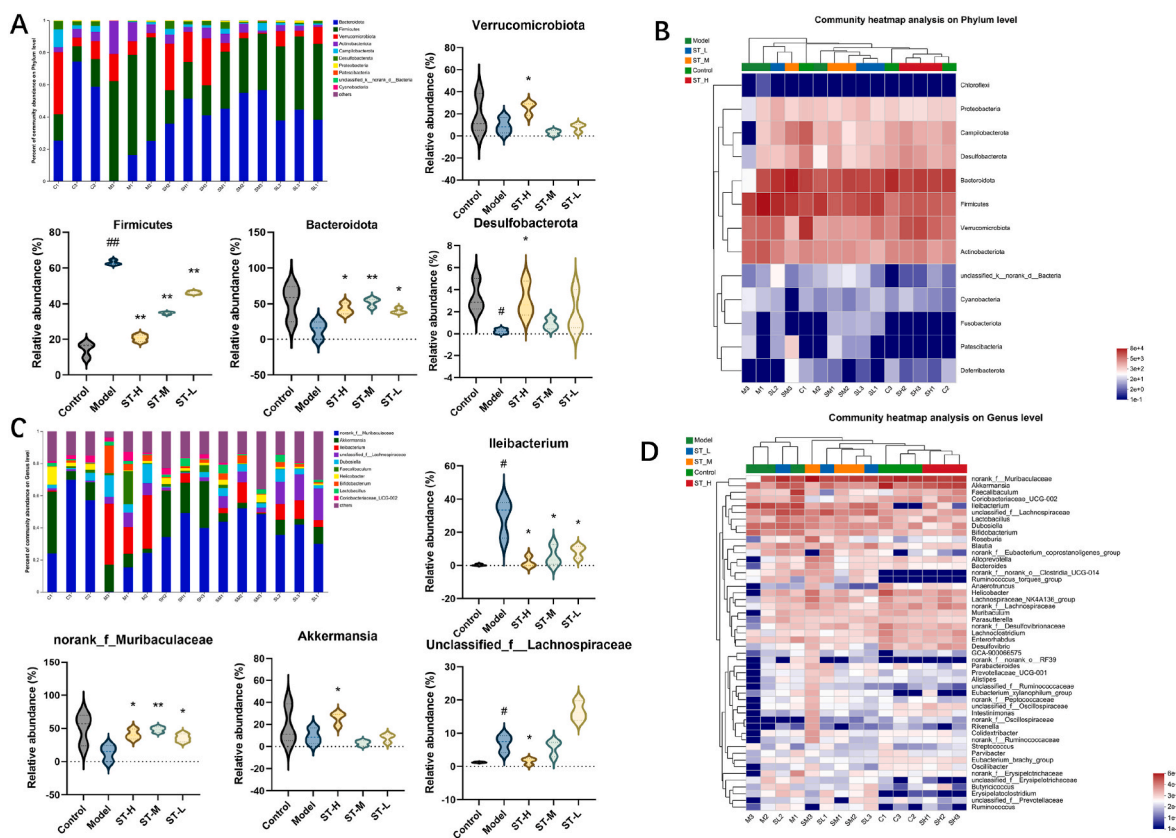


Fig. 4. The fecal bacterial community at the (A) phylum and (C) genus levels. Relative abundance heatmaps at (B) phylum and (D) genus levels. Less than 5% abundance of the phylum or genus was merged into others.

groups.

We identified specific bacterial taxa among different populations using the linear discriminant analysis effect size (LEfSe) method. Due to extensive data, we focused on performing a complex statistical analysis from the phylum to genus level considering the number of OTUs detected in this study. Groupings of cladograms (LDA scores >2) represent significant differences (Fig. 5H). The results displayed in Fig. 5I highlight the most significantly differentiated bacteria in each group. For instance, in the control group, *gHarryflintia* showed notable differentiation, while in the model group, *p\_Firmicutes* demonstrated significant distinction. However, *gLachnoclostridium* showed striking differentiation in the ST-H group, and *gCandidatusSaccharimonas* exhibited substantial differentiation in the ST-M group, *f\_Lachnospiraceae* exhibited substantial differentiation in the ST-L group. These findings shed light on the specific bacterial taxa contributing to the observed differences among study groups.

To annotate the function of the gut microbiota, we employed PIC-RUST2 functional predictions, which covered species and their functional relationships based on KEGG. Then, we compared the available forecasts for the gut using a *t*-test and generated graphs to illustrate changes in microbiota between different groups. In Fig. 6A, the study results indicated significant differences in carbohydrate metabolism, amino acid metabolism, and global and overview maps when comparing the control and model groups. Fig. 6B shows that the ST-H group also exhibited significant changes in amino acid metabolism, carbohydrate metabolism, and global and overview maps compared to the model group. These findings provide insights into the functional alterations in the gut microbiota between the control and model group and between the model and ST-H group. The differences in metabolic pathways and functional activities shed light on the potential mechanisms underlying therapeutic effects of ST-H on the model group.

### 3.5. Effect of ST on the metabolic pathways and correlation analysis of gut microbiota in HFD mice

We performed Spearman correlation analysis on the relative abundance of 12 serum metabolites and 79 microbial genera to explore the link between metabolites and the gut microbiota. We selected the top 10 serum metabolites in correlation ranking and the top 10 microbial genera in correlation ranking for screening (Fig. 6C and F). We found that vitamin A was positively correlated with *Erysipelatoclostridium*, and *Ileibacterium* etc; and negatively correlated with *Bilophila*, and *Desulfovibrio* etc. Histamine was positively correlated with *Negativibacillus* and negatively correlated with *Eubacterium brachy\_group*. Then, we selected the top 10 serum metabolites in correlation ranking and the top 4 blood lipid indices for screening (Fig. 6D and G). We found that TC was positively correlated with phenylalanine, vitamin A, and PC (18:3(9Z,12Z,15Z)/18:2(9Z,12Z)). LDL-C was positively correlated with phenylalanine, PC (18:3(9Z,12Z,15Z)/18:2(9Z,12Z)), and vitamin A. HDL-C was negatively correlated with vitamin A. Finally, we selected the top 10 intestinal microbiota in correlation ranking and the top 4 blood lipid indices for screening (Fig. 5E and H). We found that LDL-C was negatively correlated with *Desulfovibrio* and positively correlated with *Marvinbryantia*, and *Blautia* etc. TC was negatively correlated with *Lachnoclostridium*, and *Helicobacter* etc and positively correlated with *Ileibacterium* etc.

## 4. Discussion

The global trend of hyperlipidaemia is worsening, prompting medical and nutrition experts worldwide to dedicate efforts to address this problem (Saklayen, 2018). One crucial direction in treating hyperlipidaemia is the creation of functional oligosaccharides derived from natural foods to intervene in lipid metabolism (Sunarti et al., 2022;

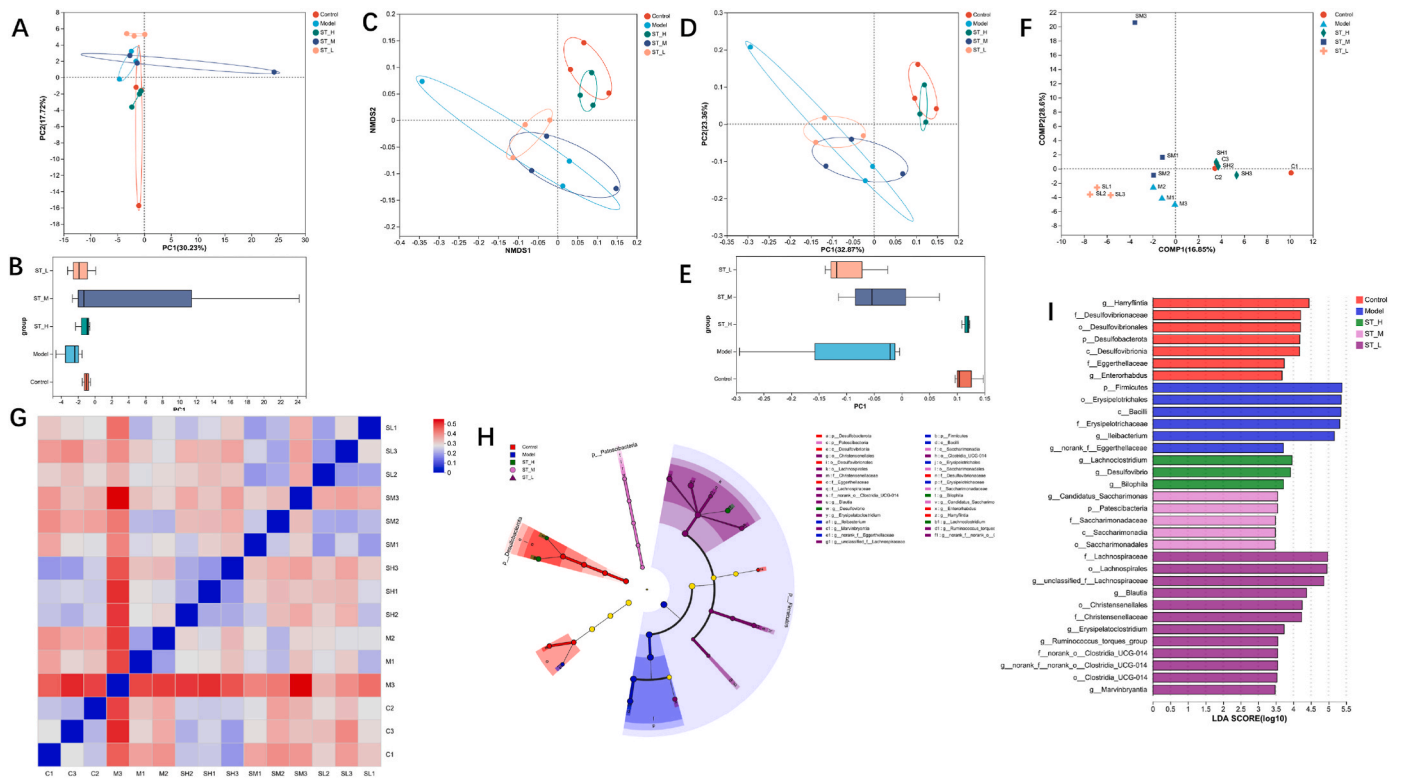


**Fig. 5.**  $\beta$ -Diversity heatmap and LefSe analysis results. (A) PCoA analysis; (B) PCoA box diagram; (C) NMDS analysis; (D) PCA analysis; (E) PCA box diagram; (F) PLS-DA analysis; (G)  $\beta$ -diversity heatmap based on unweighted uniFrac distances; (H) The indicator bacteria with an LDA score >2 in the bacterial community were associated with the five groups of mice; (I) The areas with different colors represent different components (red, control group; blue, model group; green, ST-H group; pink, ST-M group; purple, ST-L group). (For interpretation of the references to color in this figure legend, the reader is referred to the Web version of this article.)

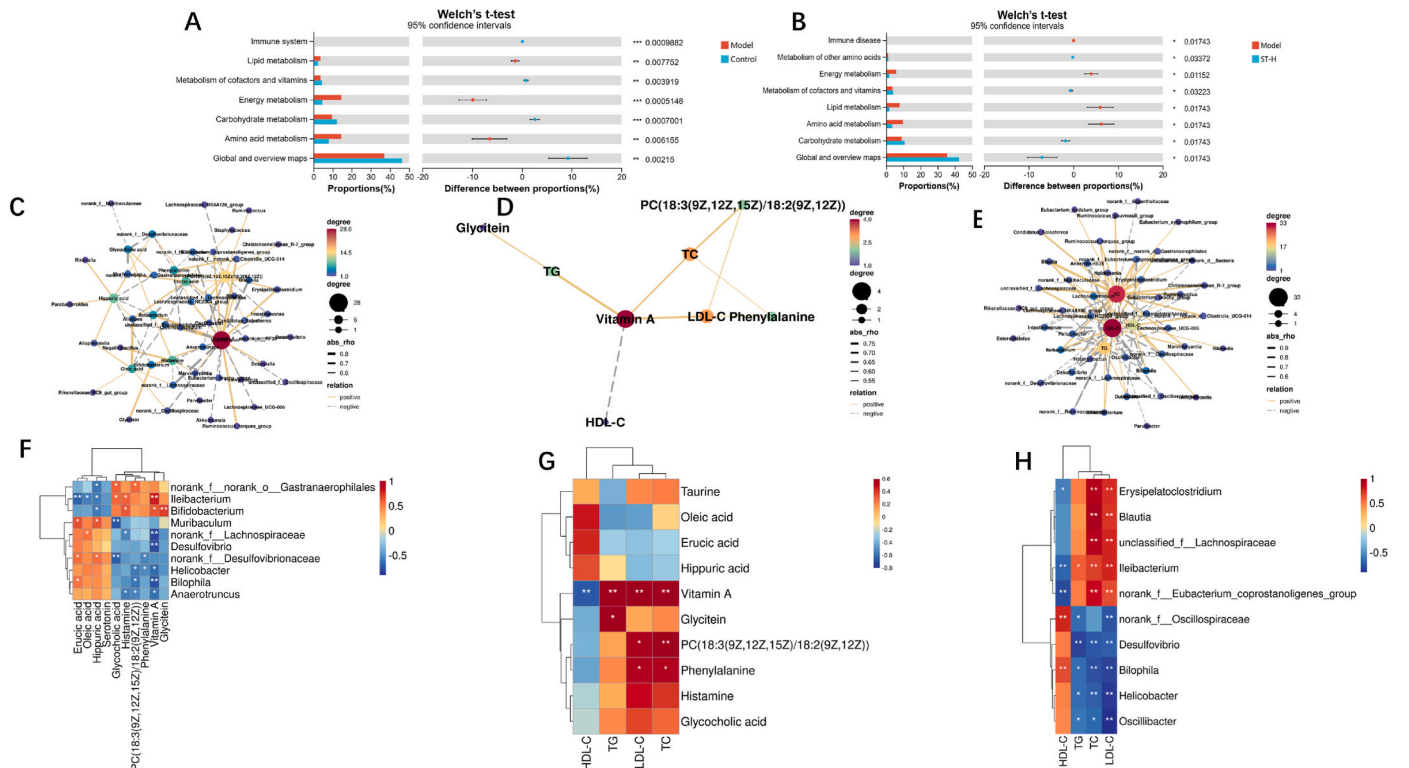


**Fig. 6.** Functional prediction of altered gut microbiota by PICRUST2 analysis based on KEGG pathways at level II in mice. (A) Control and model groups, (B) model and ST-H groups. (C) Metabolite and gut microbiota, (D) Metabolite and blood lipid, (E) gut microbiota and blood lipid correlation network diagram. (F) Metabolite and gut microbiota, (G) metabolite and blood lipid, (H) gut microbiota and blood lipid -related cluster marker heatmap.

Roberfroid, 2002; Wen et al., 2022). ST is a common oligosaccharide that plays a significant role in treating hyperlipidaemia and influences lipid metabolism (Li et al., 2016a,b). As a common food component, ST has a high safety profile and offers a broader business foundation. Despite its potential benefits, the effects of ST on hyperlipidaemia and lipid metabolism, as well as the corresponding underlying mechanisms, have yet to be thoroughly and systematically studied. To address this gap, this study is a comprehensive investigation using 16 S rRNA gene sequencing technology and metabolomics to explore the impact of ST on high-fat diet mice and the associated pathways involved.

In this study, we observed that the ST diet resulted in significant reductions in body weight, body weight gain, epididymal fat index, liver index, and blood lipid levels in HFD-induced hyperlipidaemic mice after 5 weeks. The positive effect of ST on weight management and fat accumulation was further confirmed by a significant reduction in adipocyte volume and number by H&E staining of adipose tissue, which showed a notable decrease in adipocyte volume and number. Additionally, H&E staining of liver tissue demonstrated a significant reversal in the degree of steatosis and the area of fat vacuoles, which indicated an improvement in liver health with ST feeding. Based on these collective findings, it can be concluded that ST exhibits a remarkable therapeutic effect on hyperlipidaemia and suggests its potential as a promising intervention in managing lipid disorders and associated conditions.

In recent years, the gut microbiota has emerged as a significant target for research on chronic metabolic diseases. The intestinal microbiota typically consists of billions of bacteria that maintain a symbiotic relationship with their host and play a crucial role in regulating metabolism. Many studies have emphasized that changes in the intestinal microbiota in chronic metabolic diseases are mainly characterized by an increase in *Firmicutes* and a decrease in *Bacteroidota*. The *Firmicutes* to *Bacteroidota* (F/B) ratio has thus become a critical reference marker for studying intestinal dysbiosis. In this study, utilizing 16 S rRNA sequencing, it was observed that ST intervention enhanced the gut microbiota composition in the hyperlipidaemic model mice. This enhancement was achieved by reducing the relative abundance of *Firmicutes* and increasing the relative abundance of *Bacteroidota*. These findings suggest that ST may play a role in restoring the balance of the gut microbiota and potentially contribute to its therapeutic effects on hyperlipidaemia and chronic metabolic diseases.

*Norank\_f\_Muribaculaceae* is a commonly recognized beneficial bacterium, and various studies have established a negative correlation between an increase in the relative abundance of *norank\_f\_Muribaculaceae* and diseases such as obesity and hyperlipidaemia (Song et al., 2022). *Akkermansia*, considered a probiotic, is shown in recent studies to have a beneficial effect on host health. It is crucial in regulating gut barrier function and lipid metabolism in vivo. Importantly, it protects the host's intestinal mucosal barrier and epithelial integrity by degrading mucin. Therefore, the inactivation and reduction of *Akkermansia* could lead to the attenuation of intestinal repairing activity and the onset of hyperlipidemic features (Duan et al., 2021). This study showed that ST-H significantly increased the relative abundance of *Akkermansia* at the genus level. This finding supports that ST can restore gut probiotic imbalances induced by HFD. By increasing beneficial bacteria such as *Akkermansia*, ST may contribute to the modulation of the gut microbiota and potentially exert positive effects in combating hyperlipidaemia and related metabolic disorders.

Indeed, prebiotics support the growth and activity of probiotic strains in the gut. Prebiotics were first proposed by the renowned British professor Gibson in 1995 (Gibson and Roberfroid, 1995). Prebiotics have been shown to be essential functional factors in regulating the human body's microecology and maintaining gastrointestinal tract homeostasis. They have also been recognized in preventing and treating various chronic diseases. Probiotics currently include oligosaccharides, dietary fibre, inulin, and others (Ferrarese et al., 2018). These prebiotics promote the rapid growth of specific beneficial bacteria in the intestinal tract, which helps improve gut health and overall well-being. ST is a

member of the raffinose family of oligosaccharides and consists of two  $\alpha$ -galactose sugars bonded to a 1,6-glycosidic bond on the glucose side of sucrose (Liu et al., 2018). Based on these findings, it can be concluded that ST's ability to regulate the gut microbiota imbalance induced by a HFD is attributed to its rich prebiotic properties. ST contributes to the health promotion of mice with HFD-induced conditions by providing a favourable environment for beneficial bacteria to thrive.

Research has shown that the gut microbiota metabolizes essential amino acids and aromatic amino acids, such as phenylalanine, tyrosine, and tryptophan, into various physiologically active aromatic acids. Additionally, the intestinal microbiota imbalance in the metabolism of phenylalanine, tyrosine, and tryptophan may lead to various metabolic diseases including type 2 diabetes and hyperlipidaemia (Zou et al., 2021). Elevated plasma levels of aromatic amino acids, particularly phenylalanine and tyrosine, have been observed in type 1 diabetic patients (Mathew et al., 2019). Hippuric acid and phenacetic acid, which are catabolites of phenylalanine, have nephrotoxic properties (Gu et al., 2017). However, we observed a significant decrease in phenylalanine and hippuric acid levels after undergoing ST treatment. Therefore, hippuric acid and phenylalanine have emerged as potential targets for ST in treating hyperlipidaemia.

After thoroughly analysing the potential enrichment pathways related to various metabolites using the KEGG database, we identified the top-ranked pathways as primary bile acid biosynthesis and phenylalanine metabolism. Additionally, the abundance analysis of the intestinal microbiota revealed the involvement of amino acid metabolism in the results. By correlating the differentially abundant metabolites with gut microbes at the genus level, significant associations were observed between the differential microbiota and almost all differentially abundant metabolites. As a result, it can be inferred that the beneficial effects of ST on hyperlipidaemic mice are likely attributed to the amelioration of intestinal microbial disturbances and the consequent changes in metabolic pathways and differentially abundant metabolites. A notable study finding was the significant reversal of some differentially abundant metabolites, such as taurochenodeoxycholic acid and taurine, through ST intervention. This suggests that targeting these metabolites may offer a promising approach for intervening in hyperlipidaemia. Overall, this study indicates that protective effects of ST on hyperlipidaemia may be attributed to the modulation of intestinal microbiota, alterations in metabolic pathways, and the influence on specific metabolites. These findings highlight the potential of ST as a therapeutic intervention for hyperlipidaemia and provides valuable insights into the underlying mechanisms of its action.

The findings of this study indicate that phenylalanine metabolism and primary bile acid biosynthesis are the main pathways of ST intervening in hyperlipidaemia. Clarifying this research goal can provide important information on the feasibility and benefits of ST as a potential drug or treatment in clinical applications. This helps reduce patients' symptoms of diseases caused by hyperlipidaemia and improves their quality of life.

## 5. Conclusion

In summary, our study revealed the various ameliorative effects of ST on hyperlipidaemia, including the improvement of liver function and alleviation of blood lipid levels and pathological changes. The mechanism by which ST treats hyperlipidaemia may be related to improving intestinal microbiota imbalance and regulating phenylalanine metabolism and primary bile acid biosynthesis.

## Ethics statement

The animal study was reviewed and approved by Ethics Committee of Heilongjiang University of Chinese Medicine.

## Author contributions

**HK** and **QW**: Funding acquisition; **WZ**: conceptualization, methodology, software, and data curation, writing–original draft preparation; **NC**: Writing - original draft.

## Funding

Chief Scientist of Qi-Huang Project of National Traditional Chinese Medicine Inheritance and Innovation “One Hundred Million” Talent Project (2021); Qi-Huang Scholar of National Traditional Chinese Medicine Leading Talents Support Program (2018); Heilongjiang Touyan Innovation Team Program (2019); National Famous Old Traditional Chinese Medicine Experts Inheritance Studio Construction Program of National Administration of TCM (Grant Number: [2022] No. 75); The Seventh Batch of National Famous Old Traditional Chinese Medicine Experts Experience Heritage Construction Program of National Administration of TCM (Grant Number: [2022] No. 76); This work was financially supported by Administration of Traditional Chinese Medicine of Guangdong Province, China (20221214).

## Declaration of competing interest

The authors declare that they have no known competing financial interests or personal relationships that could have appeared to influence the work reported in this paper.

## Data availability

The data that has been used is confidential.

## Appendix A. Supplementary data

Supplementary data to this article can be found online at <https://doi.org/10.1016/j.crfs.2023.100638>.

## References

- Chai, Z., Yan, Y., Zan, S., Meng, X., Zhang, F., 2022. Probiotic-fermented blueberry pomace alleviates obesity and hyperlipidemia in high-fat diet C57BL/6J mice. *Food Res. Int.* 157, 111396.
- Chen, S., Zhou, Y., Chen, Y., Gu, J., 2018. fastp: an ultra-fast all-in-one FASTQ preprocessor. *Bioinformatics* 34 (17), i884–i890. <https://doi.org/10.1093/bioinformatics/bty560>.
- Cui, N., Zhang, W., Su, F., Zhang, Z., Qiao, W., Sun, Y., Yang, B., Kuang, H., Wang, Q., 2023. Metabolomics and lipidomics study unveils the impact of tauroursodeoxycholic acid on hyperlipidemic mice. *Molecules* 28 (17), 6352. <https://doi.org/10.3390/molecules28176352>.
- Dong, Y., Zhang, J., Gao, Z., Zhao, H., Sun, G., Wang, X., Jia, L., 2019. Characterization and anti-hyperlipidemia effects of enzymatic residue polysaccharides from *Pleurotus ostreatus*. *Int. J. Biol. Macromol.* 129, 316–325. <https://doi.org/10.1016/j.ijbiomac.2019.01.164>.
- Duan, R., Guan, X., Huang, K., Zhang, Y., Li, S., Xia, J., Shen, M., 2021. Flavonoids from whole-grain oat alleviated high-fat diet-induced hyperlipidemia via regulating bile acid metabolism and gut microbiota in mice. *J. Agric. Food Chem.* 69 (27), 7629–7640. <https://doi.org/10.1021/acs.jafc.1c01813>.
- Edgar, R.C., 2013. UPARSE: highly accurate OTU sequences from microbial amplicon reads. *Nat. Methods* 10 (10), 996–998. <https://doi.org/10.1038/nmeth.2604>.
- Ferrarese, R., Ceresola, E.R., Preti, A., Canducci, F., 2018. Probiotics, prebiotics and synbiotics for weight loss and metabolic syndrome in the microbiome era. *Eur. Rev. Med. Pharmacol. Sci.* 22 (21), 7588–7605.
- Gibson, G.R., Roberfroid, M.B., 1995. Dietary modulation of the human colonic microbiota: introducing the concept of prebiotics. *J. Nutr.* 125 (6), 1401–1412.
- Gu, L., Shi, H., Zhang, R., Wei, Z., Bi, K.S., Chen, X.H., 2017. Simultaneous determination of five specific and sensitive nephrotoxicity biomarkers in serum and urine samples of four drug-induced kidney injury models. *J. Chromatogr. Sci.* 55 (1), 60–68.
- Jovanovic-Malinovska, R., Kuzmanova, S., Winkelhausen, E., 2015. Application of ultrasound for enhanced extraction of prebiotic oligosaccharides from selected fruits and vegetables. *Ultrason. Sonochem.* 22, 446–453.
- Li, W., Huang, D., Gao, A., Yang, X., 2016a. Stachyose increases absorption and hepatoprotective effect of tea polyphenols in high fructose-fed mice. *Mol. Nutr. Food Res.* 60 (3), 502–510.
- Li, W., Li, Z., Han, X., Huang, D., Lu, Y., Yang, X., 2016b. Enhancing the hepatic protective effect of genistein by oral administration with stachyose in mice with chronic high fructose diet consumption. *Food Funct.* 7 (5), 2420–2430.
- Liu, C., Zhao, D., Ma, W., Guo, Y., Wang, A., Wang, Q., Lee, D.J., 2016. Denitrifying sulfide removal process on high-salinity wastewaters in the presence of *Halomonas* sp. *Appl. Microbiol. Biotechnol.* 100 (3), 1421–1426. <https://doi.org/10.1007/s00253-015-7039-6>.
- Liu, G., Bei, J., Liang, L., Yu, G., Li, L., Li, Q., 2018. Stachyose improves inflammation through modulating gut microbiota of high-fat diet/streptozotocin-induced type 2 diabetes in rats. *Mol. Nutr. Food Res.* 62 (6), e1700954.
- Liu, P., Wang, Z.H., Kang, S.S., Liu, X., Xia, Y., Chan, C.B., Ye, K., 2022. High-fat diet-induced diabetes couples to Alzheimer’s disease through inflammation-activated C/EBP $\beta$ /AEP pathway. *Mol. Psychiatr.* 27 (8), 3396–3409.
- Liu, Y., Li, T., Alim, A., Ren, D., Zhao, Y., Yang, X., 2019. Regulatory effects of stachyose on colonic and hepatic inflammation, gut microbiota dysbiosis, and peripheral CD4<sup>+</sup> T cell distribution abnormality in high-fat diet-fed mice. *J. Agric. Food Chem.* 67 (42), 11665–11674.
- Lu, Y., Lin, D., Li, W., Yang, X., 2017. Non-digestible stachyose promotes bioavailability of genistein through inhibiting intestinal degradation and first-pass metabolism of genistein in mice. *Food Nutr. Res.* 61 (1), 1369343.
- Magoč, T., Salzberg, S.L., 2011. FLASH: fast length adjustment of short reads to improve genome assemblies. *Bioinformatics* 27 (21), 2957–2963. <https://doi.org/10.1093/bioinformatics/btr507>.
- Mathew, A.V., Jaiswal, M., Ang, L., Michailidis, G., Pennathur, S., Pop-Busui, R., 2019. Impaired amino acid and TCA metabolism and cardiovascular autonomic neuropathy progression in type 1 diabetes. *Diabetes* 68 (10), 2035–2044.
- Nasioudis, D., Doulaveris, G., Kanninen, T.T., 2019. Dyslipidemia in pregnancy and maternal-fetal outcome. *Minerva Ginecol.* 71 (2), 155–162.
- Olsson, M.E., Ekvall, J., Gustavsson, K.E., Nilsson, J., Pillai, D., Sjöholm, I., Svensson, U., Akesson, B., Nyman, M.G., 2004. Antioxidants, low molecular weight carbohydrates, and total antioxidant capacity in strawberries (*Fragaria x ananassa*): effects of cultivar, ripening, and storage. *J. Agric. Food Chem.* 52 (9), 2490–2498.
- Roberfroid, M.B., 2002. Functional foods: concepts and application to inulin and oligofructose. *Br. J. Nutr. Suppl.* 2, S139–S143.
- Saklayen, M.G., 2018. The global epidemic of the metabolic syndrome. *Curr. Hypertens. Rep.* 20 (2), 12.
- Song, Y., Cai, Q., Wang, S., Li, L., Wang, Y., Zou, S., Gao, X., Wei, Y., 2022. The ameliorative effect and mechanisms of *Ruditapes philippinarum* bioactive peptides on obesity and hyperlipidemia induced by a high-fat diet in mice. *Nutrients* 14 (23), 5066. <https://doi.org/10.3390/nu14235066>.
- Sunarti, Mumpuni, H., Yasmine, N., Marsono, Y., Fibri, D.L.N., Murdiati, A., 2022. FiberCrema as a functional food ingredient reduces hyperlipidemia and risk of cardiovascular diseases in subjects with hyperlipidemia. *Prev. Nutr. Food Sci.* 27 (2), 165–171.
- Tietge, U.J., 2014. Hyperlipidemia and cardiovascular disease: inflammation, dyslipidemia, and atherosclerosis. *Curr. Opin. Lipidol.* 25 (1), 94–95.
- Tóth, M.E., Dukay, B., Hoyk, Z., Sántha, M., 2020. Cerebrovascular changes and neurodegeneration related to hyperlipidemia: characteristics of the human ApoB-100 transgenic mice. *Curr. Pharmaceut. Des.* 26 (13), 1486–1494.
- Wen, F., Wang, F., Li, P., Shi, H., Liu, N., 2022. Effect of xylo-oligosaccharides on reproduction, lipid metabolism, and adipokines of hens during the late egg-laying period. *Animal bioscience* 35 (11), 1744–1751.
- Yoo, W., Zieba, J.K., Foegeding, N.J., Torres, T.P., Shelton, C.D., Shealy, N.G., Byndloss, A.J., Cevallos, S.A., Gertz, E., Tiffany, C.R., Thomas, J.D., Litvak, Y., Nguyen, H., Olsan, E.E., Bennett, B.J., Rathmell, J.C., Major, A.S., Bäuml, A.J., Byndloss, M.X., 2021. High-fat diet-induced colonocyte dysfunction escalates microbiota-derived trimethylamine N-oxide. *Science* 373 (6556), 813–818.
- Yu, X., Meng, X., Yan, Y., Wang, H., Zhang, L., 2022a. Extraction of naringin from pomelo and its therapeutic potentials against hyperlipidemia. *Molecules* 27 (24), 9033. <https://doi.org/10.3390/molecules27249033>.
- Yu, Z., Qin, E., Cheng, S., Yang, H., Liu, R., Xu, T., Liu, Y., Yuan, J., Yu, S., Yang, J., Liang, F., 2022b. Gut microbiome in PCOS associates to serum metabolomics: a cross-sectional study. *Sci. Rep.* 12 (1), 22184.
- Zou, B., Sun, Y., Xu, Z., Chen, Y., Li, L., Lin, L., Zhang, S., Liao, Q., Xie, Z., 2021. Rapid simultaneous determination of gut microbial phenylalanine, tyrosine, and tryptophan metabolites in rat serum, urine, and faeces using LC-MS/MS and its application to a type 2 diabetes mellitus study *Biomedical chromatography: BMC*, 35 (2), e4985.